Supporting Information

Optimizing ammonium vanadate crystal structure by facile in-situ phase transformation of $VO_2/NH_4V_4O_{10}$ with special micro-nano feature for advanced aqueous zinc ion batteries

Liming Chen[a,1], Yu Zheng[a,c,1], Ziqiang Zhang[a], Yu Ma[a], Yuanming Wang[b,] **, Huanhao, Xiao[a], Ming Xu[a], Zikun Li[c,] *** and Guohui Yuan[a,] *

[a] MIIT Key Laboratory of Critical Materials Technology for New Energy Conversion and Storage, School of Chemistry and Chemical Engineering, Harbin Institute of Technology, Harbin 150001, P. R. China

[b] College of Bioresources Chemical and Materials Engineering, Shaanxi Provincial Key Laboratory of Papermaking Technology and Specialty Paper Development, National Demonstration Center for Experimental Light Chemistry Engineering Education, Shaanxi University of Science & Technology, Xi'an 710021, P. R. China

[c] BTR New Material Group Co., Ltd., Shenzhen 518106, P. R. China

*Corresponding author at: School of Chemistry and Chemical Engineering, Harbin Institute of Technology, Harbin 150001, P. R. China

**Corresponding author at: College of Bioresources Chemical and Materials Engineering, Shaanxi University of Science & Technology, Xi'an 710021, P. R. China

***Corresponding author at: BTR New Material Group Co., Ltd., Shenzhen 518106, P. R. China

1. These authors contributed equally to this work.

E-mail addresses: yghhit@163.com (G. Yuan), ymighit@163.com (Y. Wang), lizikun@btrchina.com (Z. Li).

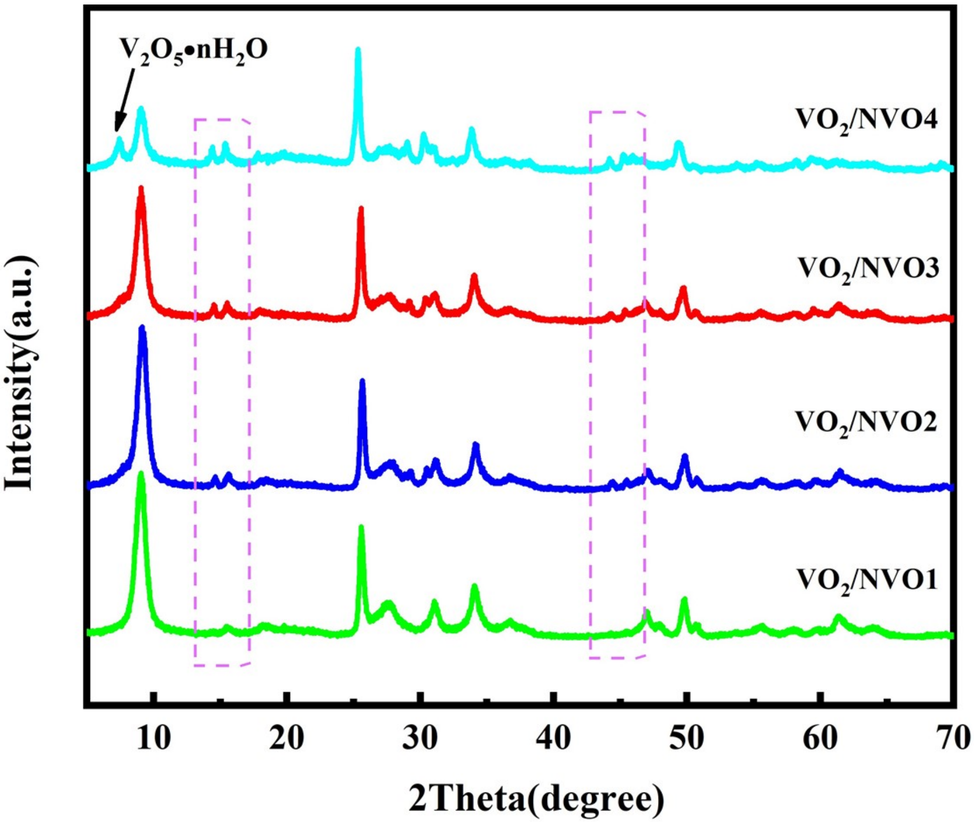

Figure S1.XRD of VO_2/NVO1, VO_2/NVO2, VO_2/NVO3 and VO_2/NVO4.

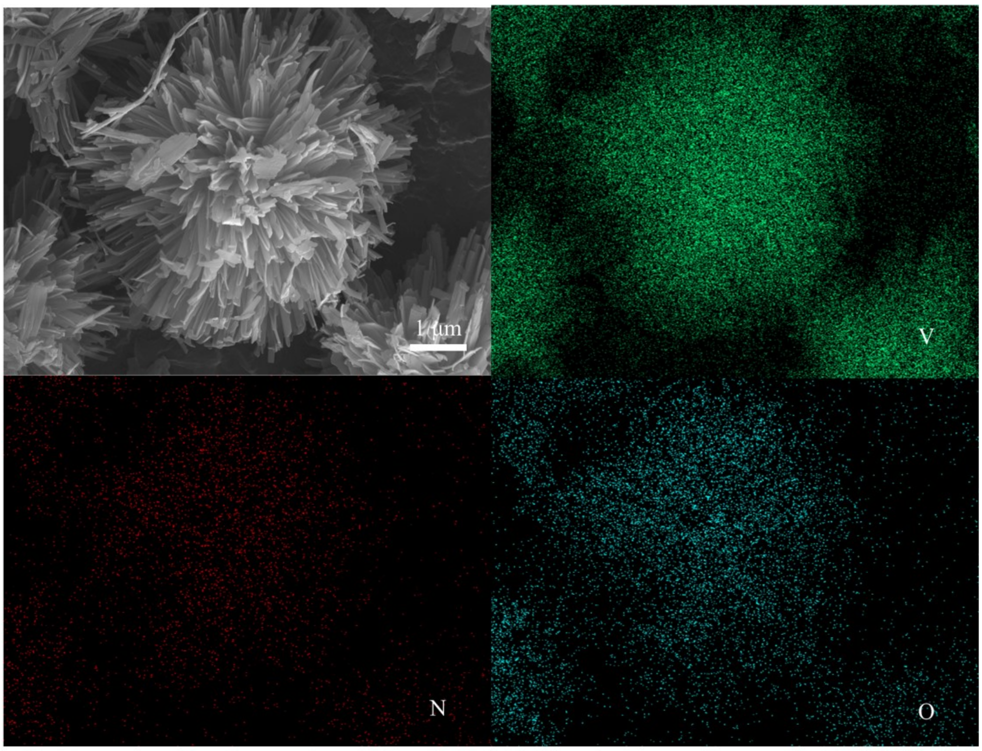

Figure S2. SEM and corresponding EDS mapping for VO_2/NVO3.

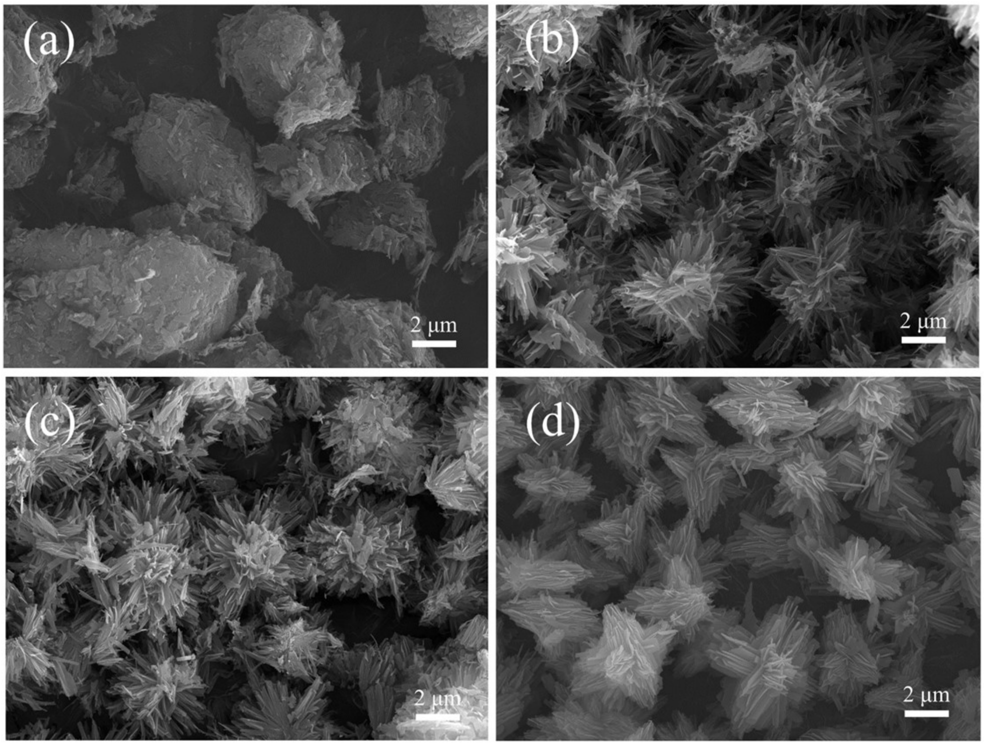

Figure S3. SEM images of (a) $NH_4V_4O_{10}$, (b) VO_2/NVO1, (c) VO_2/NVO2 and (d) VO_2/NVO4.

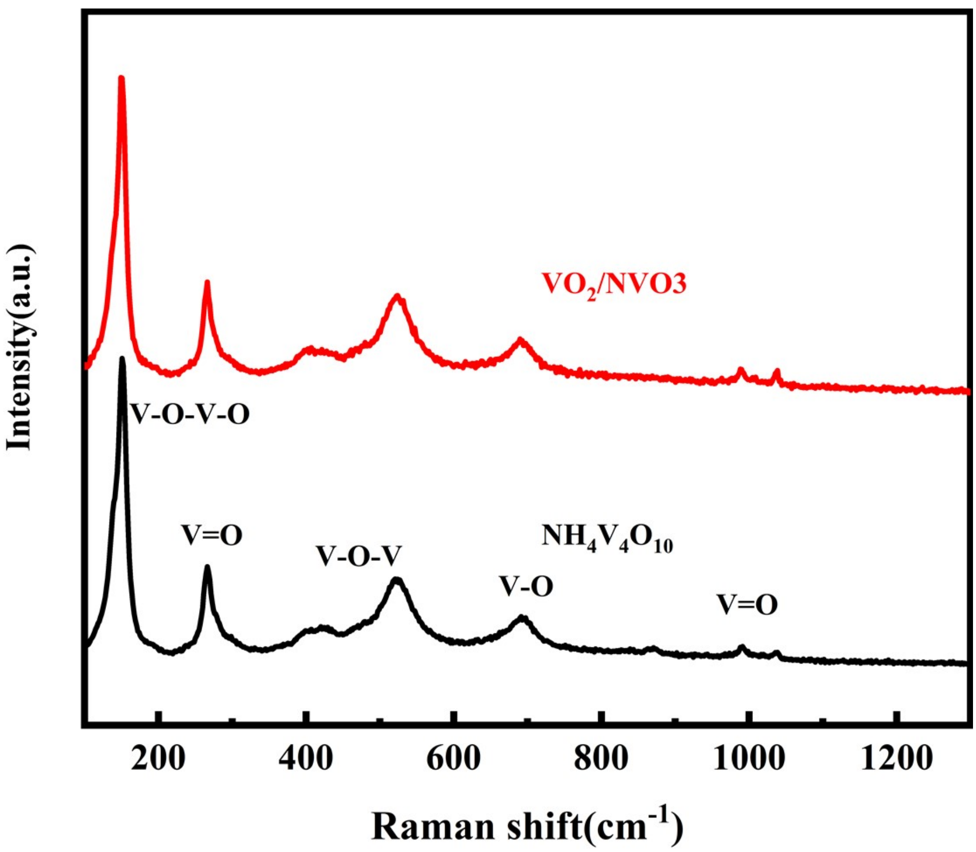

Figure S4. Raman spectrum of $NH_4V_4O_{10}$ and VO_2/NVO3.

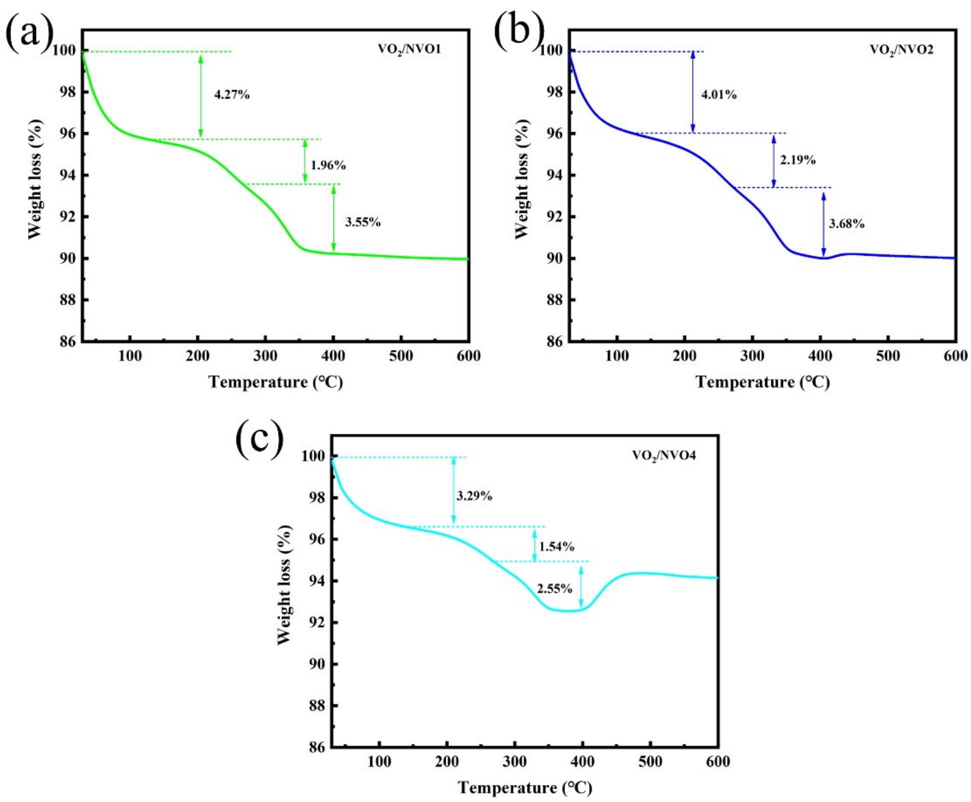

Figure S5. (a-c) TG curves of VO_2/NVO1, VO_2/NVO2 and VO_2/NVO4 materials.

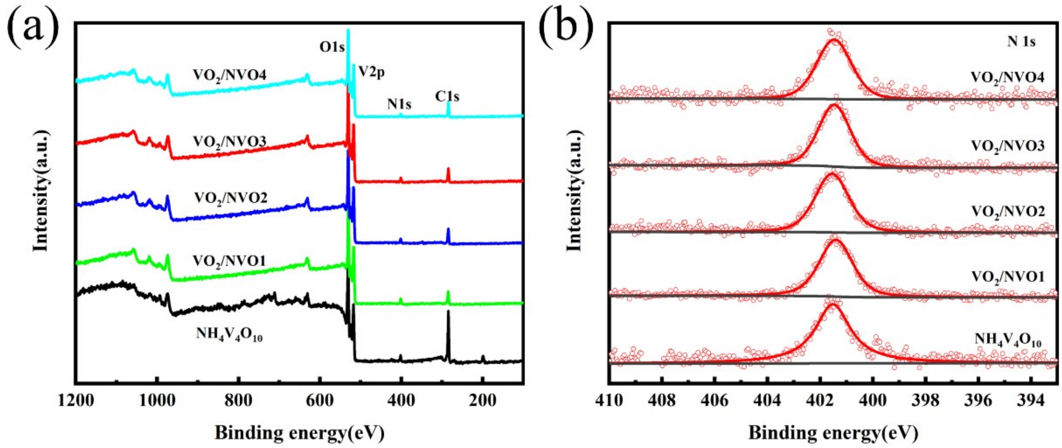

Figure S6. (a) XPS spectrum and (b) N 1s high-resolution of $NH_4V_4O_{10}$, VO_2/NVO1, VO_2/NVO2, VO_2/NVO3 and VO_2/NVO4 materials.

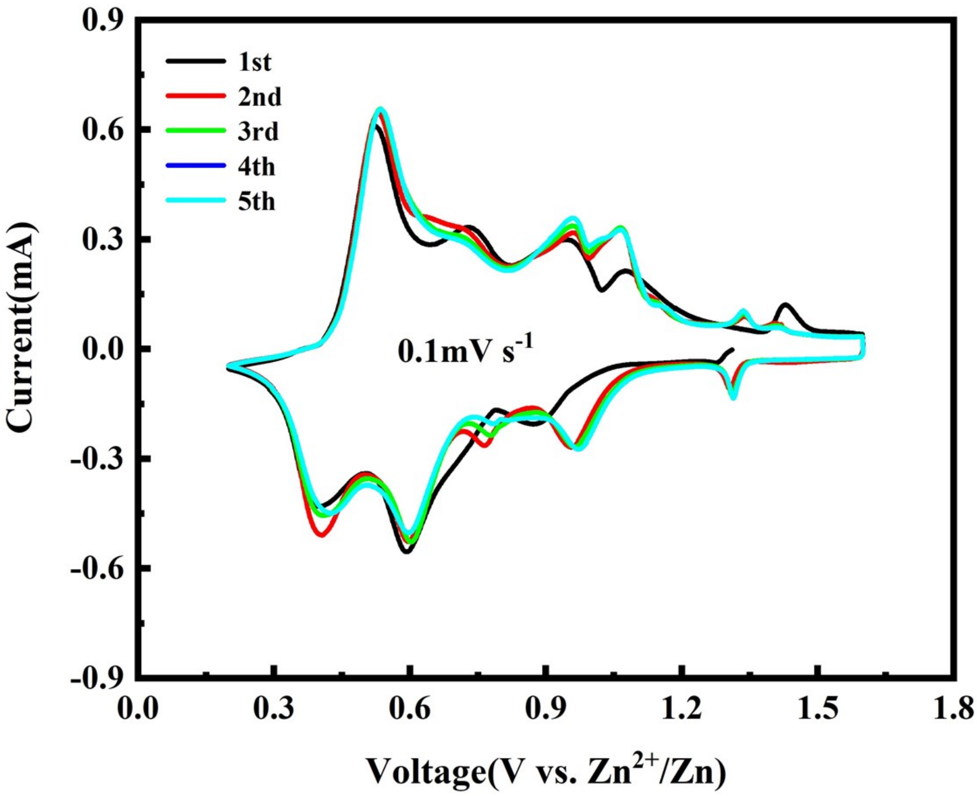

Figure S7. The first five CV curves of $NH_4V_4O_{10}$ electrodes at 0.1 mV s^{-1}.

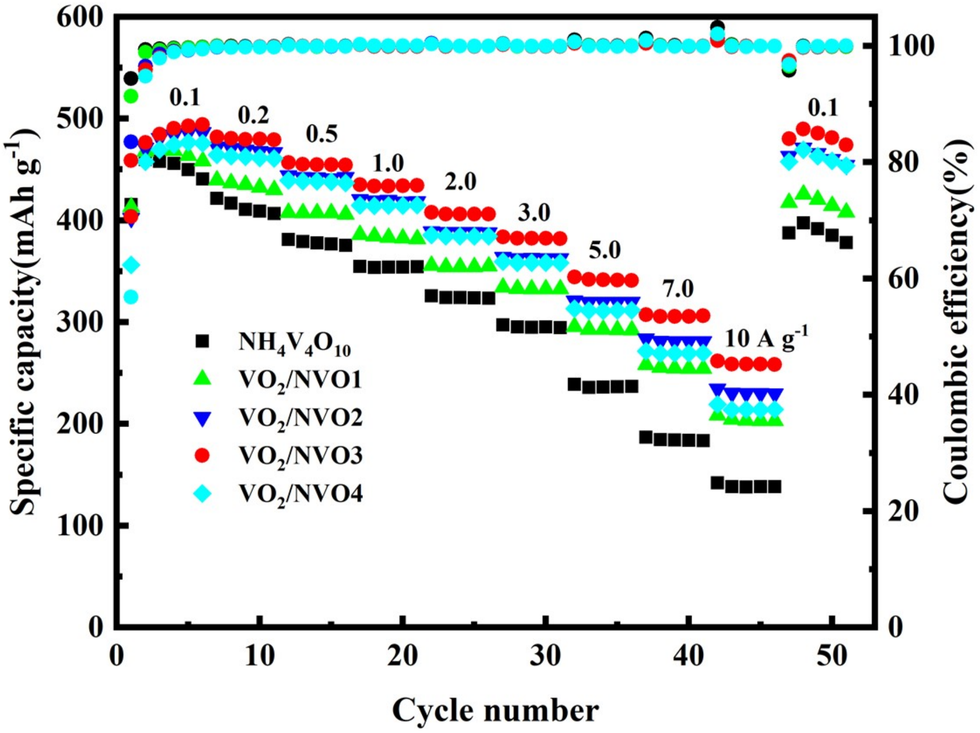

Figure S8. Rate performance of $NH_4V_4O_{10}$, VO_2/NVO1, VO_2/NVO2, VO_2/NVO3 and VO_2/NVO4 electrodes.

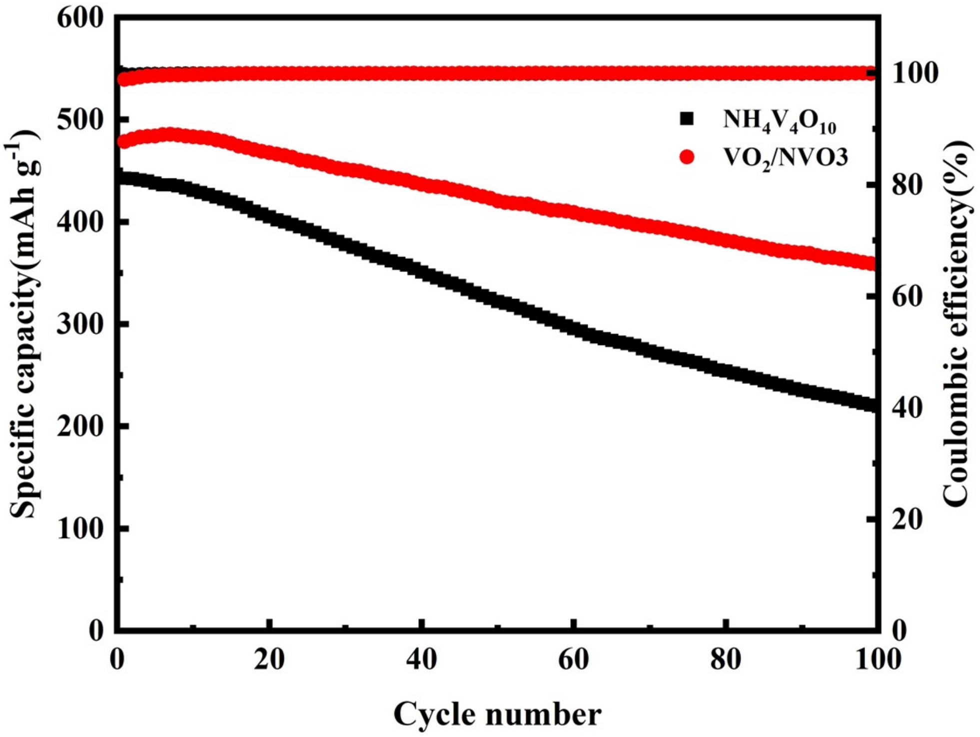

Figure S9. Cycle performance of $NH_4V_4O_{10}$ and VO_2/NVO3 electrodes at 0.2 A g^{-1}.

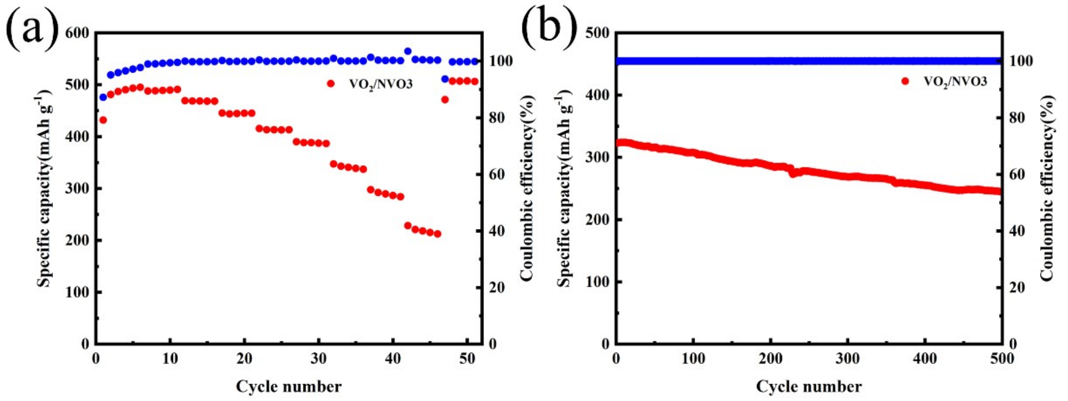

Figure S10. (a) Rate performance at various current density and (b) cycle performance at 5 Ag^{-1} of the VO_2/NVO3 electrode with high loading mass of 6 mg cm^{-2}.

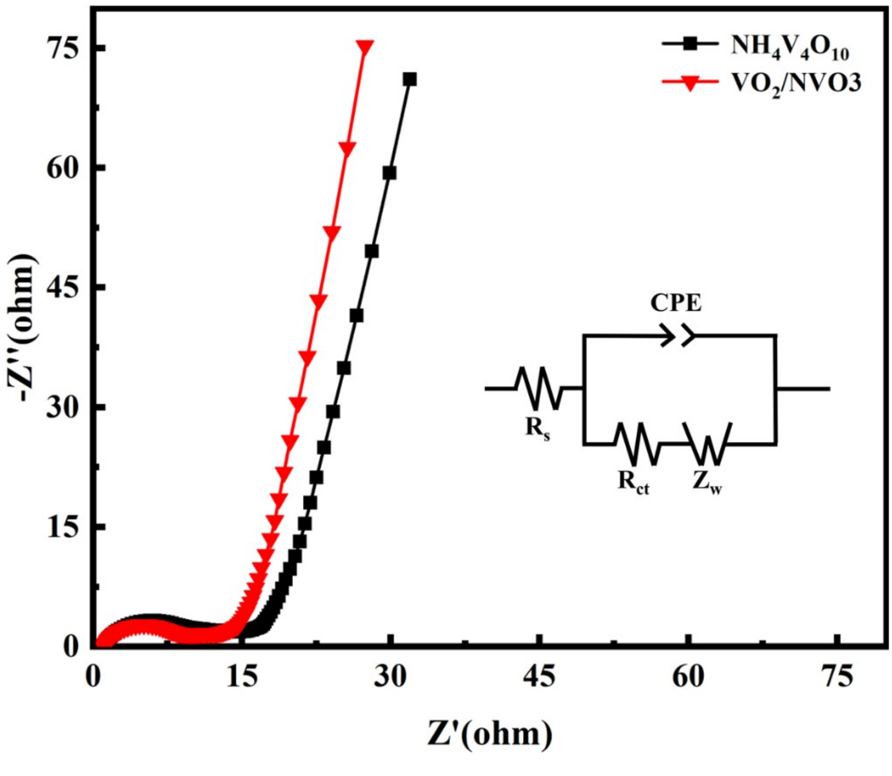

Figure S11. EIS curves of $NH_4V_4O_{10}$, VO_2/NVO1, VO_2/NVO2, VO_2/NVO3 and VO_2/NVO4 electrodes.

GITT: The battery was discharged or charged for 10 min at the current density of 0.1A g^{-1}, followed by relaxation for 60 min to back to equilibrium. And the Zn^{2+}

diffusion coefficient ($D_{Zn^{2+}}$) was calculated by the galvanostatic and intermittent titration technique (GITT), which was based on the following equation:

$$D_{Zn^{2+}} = \frac{4}{\pi\tau}\left(\frac{m_B V_M}{M_B S}\right)^2\left(\frac{\Delta E_s}{\Delta E_\tau}\right)^2 \tag{S1}$$

Where τ represents current pulse time, m_B is the mass of the active material. M_B is the molecular weight (g mol^{-1}), V_M is the molar volume (cm^3 mol^{-1}) and S delegates the surface area of electrode. The ΔEτ and ΔEs correspond to the voltage change of constant current pulse and the steady-state voltage change of the current pulse, respectively.

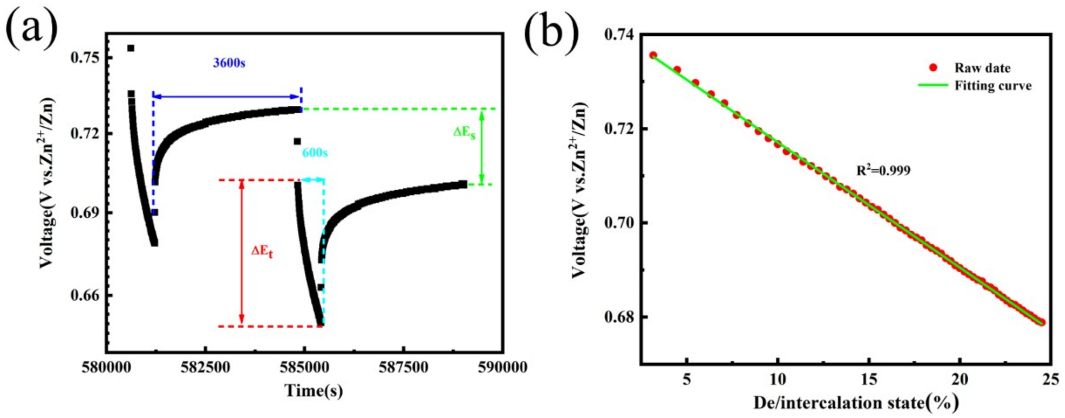

Figure S12. (a) Schematic illustration of partial enlarged GITT curve and (b) the linear relationship between E and $\tau^{1/2}$ for VO_2/NVO3 electrode.

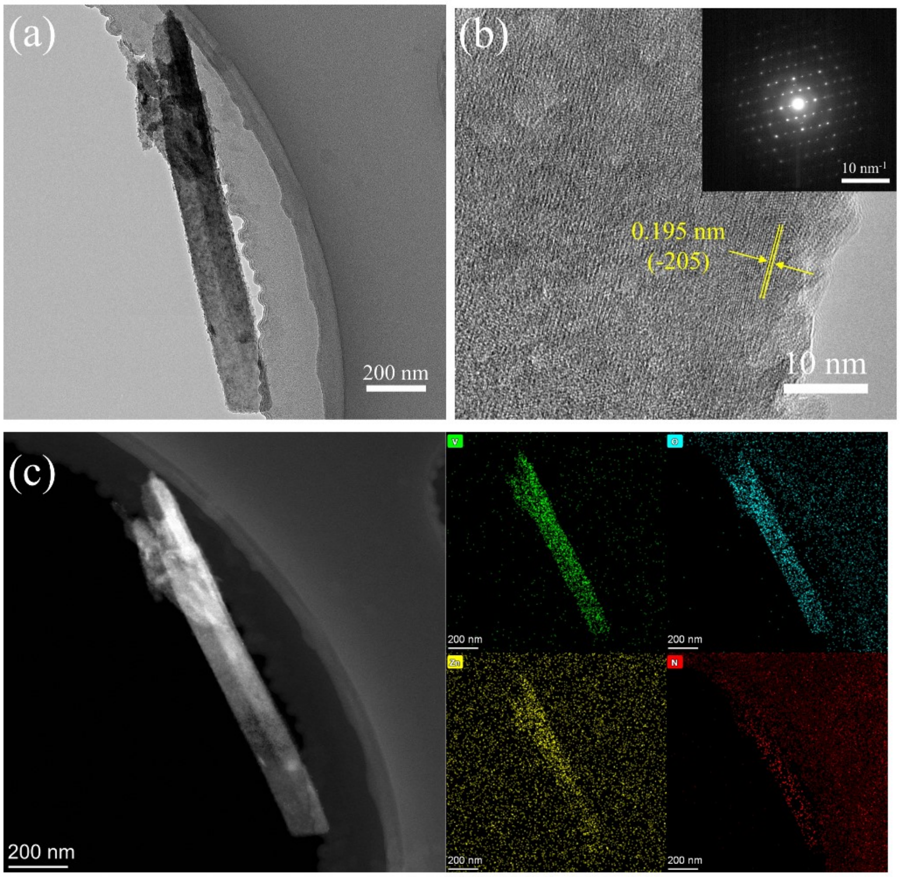

Figure S13. The TEM image of VO2/NVO3 after 3 cycles

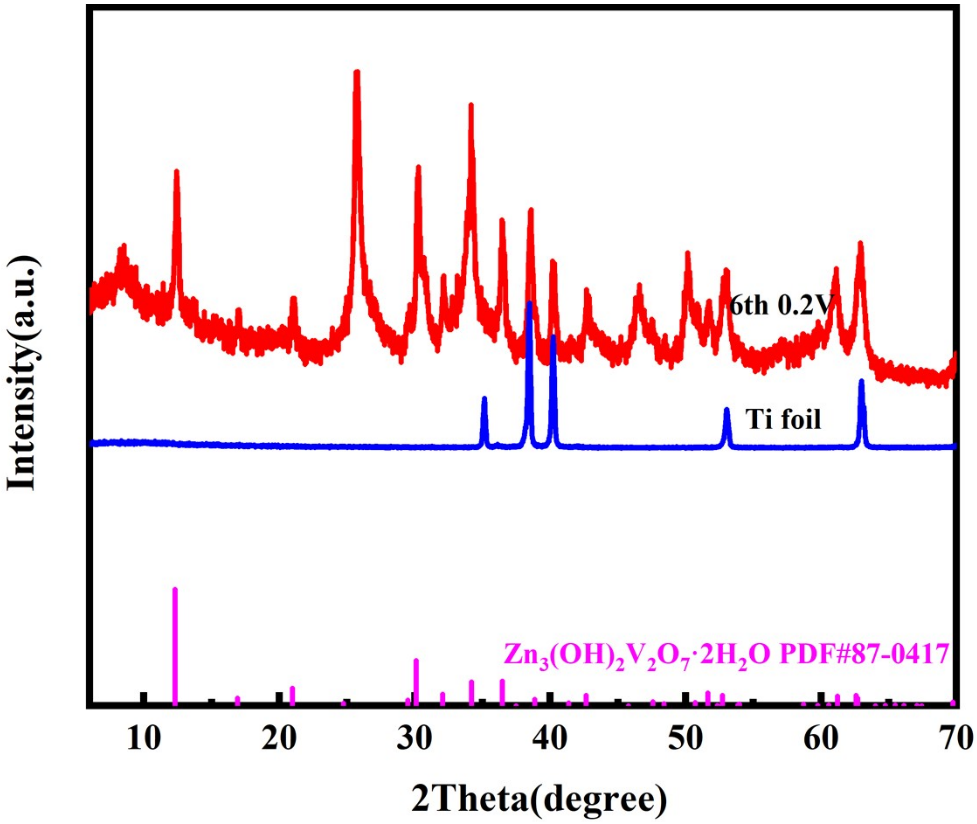

Figure S14. XRD pattern of VO_2/NVO3 electrode at 0.2 V after suffering 6 cycles.

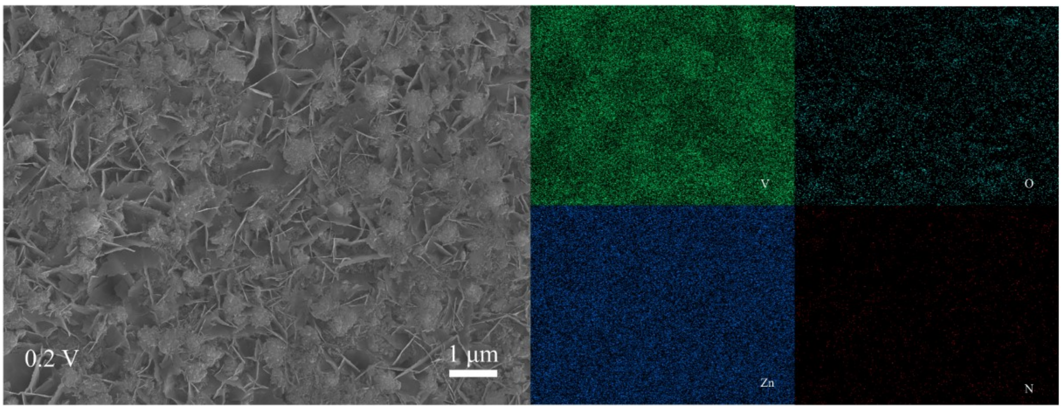

Figure S15. SEM image of VO_2/NVO3 electrode at 0.2 V after suffering 6 cycles.

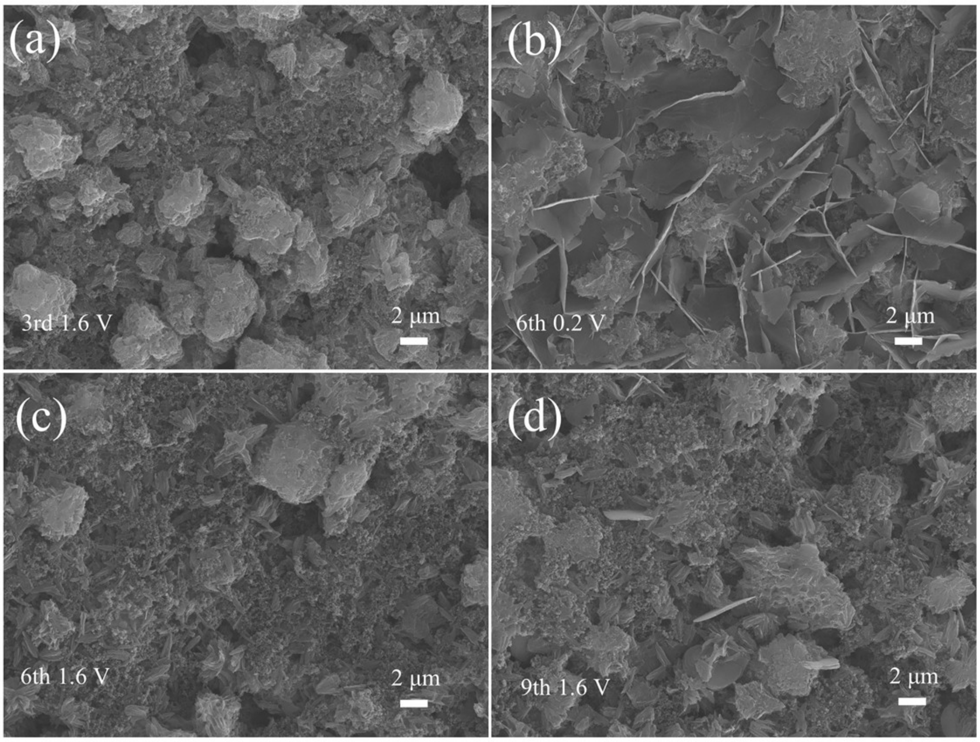

Figure S16. (a-d) SEM image of VO_2/NVO3 electrode at various charge/discharge state after different cycles.

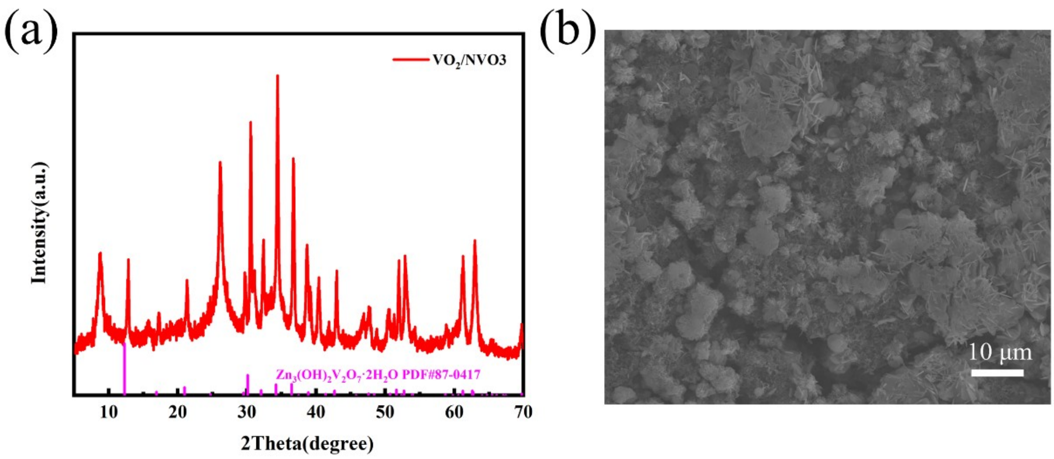

Figure S17. (a) XRD patteren and (b)SEM images of VO_2/NVO3 electrode after 1000 cycles at the current density of 5 A g^{-1}.

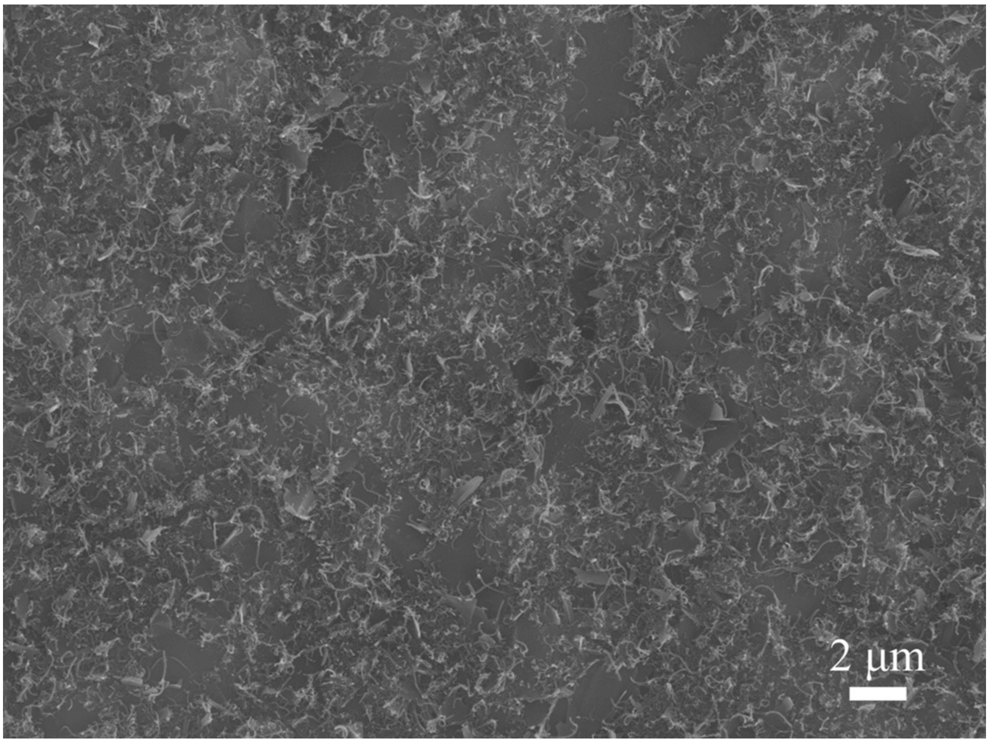

Figure S18. SEM image of VO_2/NVO3/CG electrode.

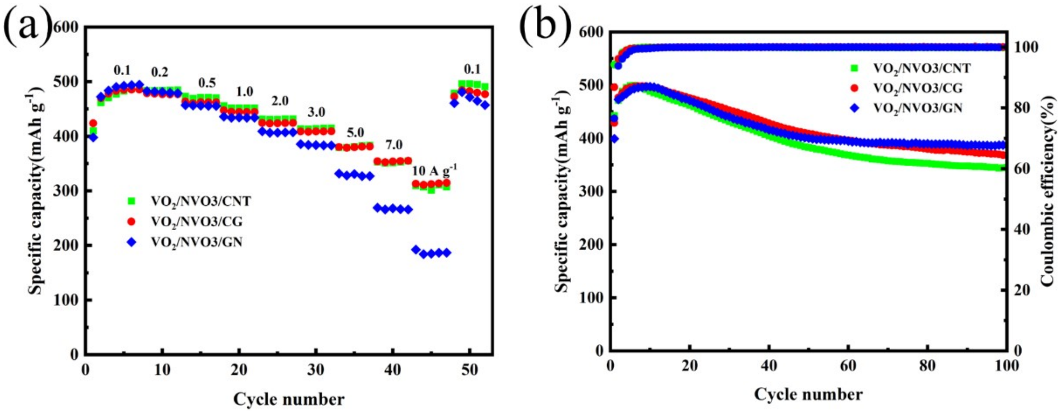

Figure S19. (a) Rate performance and (b) cycle performance at 0.1A g^{-1} of

VO_2/NVO3/CNT, VO_2/NVO3/CG and VO_2/NVO3/GN membrane electrodes.

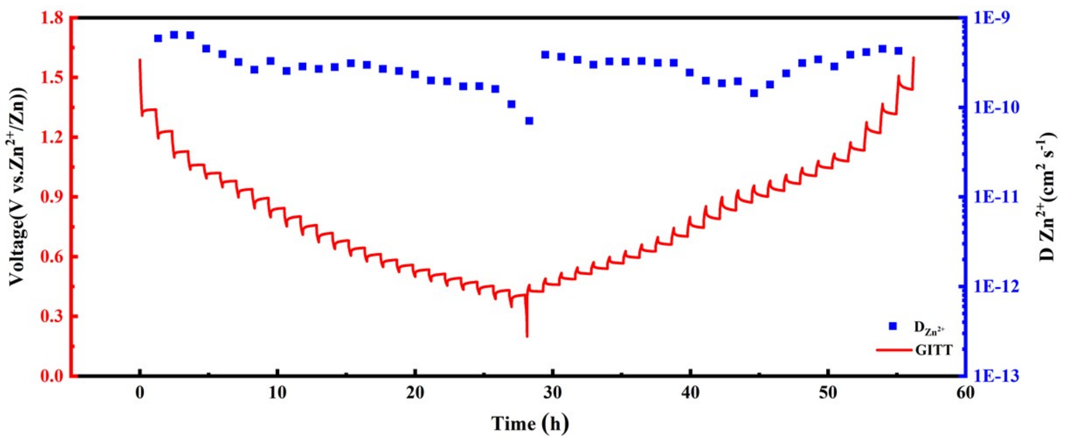

Figure S20. GITT curves and evaluated Zn^{2+} diffusion coefficient of VO_2/NVO3/CG electrode.

Table S1. The electrochemical property comparison of VO_2/NVO3 and reported vanadium based materials.

Cathode materrials	Specific capacity	Rate performance	Power density	Energy density	Ref.
$NH_4V_4O_{10-x}$/rGO	391 mAh g^{-1} at 1.0 A g^{-1}	187 mAh g^{-1} at 20 A g^{-1}	657.2 W kg^{-1}	260 Wh kg^{-1}	1
$V_2O_5·nH_2O$/PPy	383 mAh g^{-1} at 0.1 A g^{-1}	281 mAh g^{-1} at 2 A g^{-1}	95 W kg^{-1}	358 Wh kg^{-1}	2
$V_2O_5·nH_2O$/rGO	465 mAh g^{-1} at 0.1 A g^{-1}	230 mAh g^{-1} at 15 A g^{-1}	67 W kg^{-1}	312 Wh kg^{-1}	3
$H_{11}Al_2V_6O_{23.2}$	416.3 mAh g^{-1} at 0.3 A g^{-1}	138.9 mAh g^{-1} at 5 A g^{-1}	220.1 W kg^{-1}	307.4 Wh kg^{-1}	4
$K_{0.43}(NH_4)_{0.12}V_2O_{5-\delta}$	373.7 mAh g^{-1} at 0.5 A g^{-1}	216.8 mAh g^{-1} at 10 A g^{-1}	71.1 W kg^{-1}	269 Wh kg^{-1}	5
$NH_4V_4O_{10}$-300	334 mAh g^{-1} at 0.5 A g^{-1}	210 mAh g^{-1} at 10 A g^{-1}	209 W kg^{-1}	245 Wh kg^{-1}	6
$Cs_{0.24}V_2O_5·0.19H_2O$	400 mAh g^{-1} at 0.2 A g^{-1}	224 mAh g^{-1} at 20 A g^{-1}	147 W kg^{-1}	294 Wh kg^{-1}	7
$NH_4V_4O_{10}/C_3N_4$	391.6 mAh g^{-1} at 1.0 A g^{-1}	194.7 mAh g^{-1} at 20 A g^{-1}	348.6 W kg^{-1}	289.3 Wh kg^{-1}	8
Od-$VO_2·xH_2O$/PPy	346.5 mAh g^{-1} at 0.1 A g^{-1}	206 mAh g^{-1} at 10 A g^{-1}	67.6 W kg^{-1}	223 Wh kg^{-1}	9
VO_2/NVO3	493.98 mAh g^{-1} at 0.1 A g^{-1}	258.60 mAh g^{-1} at 10 A g^{-1}	72.10, 5938.85 W kg^{-1}	356.34, 155.40 Wh kg^{-1}	This work

Table S2 The comparison of Zn^{2+} diffusion coefficient of VO_2/NVO3 and previous reported V-based cathode materials.

V-based cathode materials	Zn^{2+} diffusion coefficient ($cm^2\ s^{-1}$)	References
NVO-300/CC	$10^{-12} \sim 10^{-10}$	10
Ti-NVO	$10^{-11} \sim 10^{-10}$	11
KNVO/CC	$10^{-13} \sim 10^{-11}$	12
Na-NVO	$10^{-9.2} \sim 10^{-10}$	13
$V_2O_5 \cdot nH_2O$	$10^{-8} \sim 10^{-9}$	14
$PANI_{0.22} \cdot V_2O_5 \cdot 0.88H_2O$	$10^{-8} \sim 10^{-10}$	15
$Ca_{0.24}V_2O_5$	$10^{-8} \sim 10^{-10}$	16
VO_2/NVO3	$10^{-10.1} \sim 10^{-9.6}$	This work
VO_2/NVO3/CG	$10^{-9.8} \sim 10^{-9.4}$	This work

Reference.

1. F. Cui, D. Wang, F. Hu, X. Yu, C. Guan, G. Song, F. Xu and K. Zhu, Deficiency and surface engineering boosting electronic and ionic kinetics in $NH_4V_4O_{10}$ for high-performance aqueous zinc-ion battery, *Energy Storage Mater.*, 2022, **44**, 197-205.
2. Z. Feng, J. Sun, Y. Liu, H. Jiang, T. Hu, M. Cui, F. Tian, C. Meng and Y. Zhang, Polypyrrole-intercalation tuning lamellar structure of $V_2O_5 \cdot nH_2O$ boosts fast zinc-ion kinetics for aqueous zinc-ion battery, *J. Power Sources*, 2022, **536**, 231489.
3. H. Luo, B. Wang, F. Wu, J. Jian, K. Yang, F. Jin, B. Cong, Y. Ning, Y. Zhou, D. Wang, H. Liu and S. Dou, Synergistic nanostructure and heterointerface design propelled ultra-efficient in-situ self-transformation of zinc-ion battery cathodes with favorable kinetics, *Nano Energy*, 2021, **81**, 105601.
4. L. Xing, C. Zhang, M. Li, P. Hu, X. Zhang, Y. Dai, X. Pan, W. Sun, S. Li, J. Xue, Q. An and L. Mai, Revealing excess Al^{3+} preinsertion on altering diffusion paths of aluminum vanadate for zinc-ion batteries, *Energy Storage Mater.*, 2022, **52**, 291-298.
5. Y. Zhao, S. Liang, X. Shi, Y. Yang, Y. Tang, B. Lu and J. Zhou, Synergetic Effect of Alkali-Site Substitution and Oxygen Vacancy Boosting Vanadate Cathode for Super-Stable Potassium and Zinc Storage, *Adv. Funct. Mater.*, 2022, **32**, 2203819.
6. Y. Zheng, C. Tian, Y. Wu, L. Li, Y. Tao, L. Liang, G. Yu, J. Sun, S. Wu, F. Wang, Y. Pang, Z. Shen, Z. Pan, H. Chen and J. Wang, Dual-engineering of ammonium vanadate for enhanced aqueous and quasi-solid-state zinc ion batteries, *Energy Storage Mater.*, 2022, **52**, 664-674.

7. H. Liu, X. Hou, T. Fang, Q. Zhang, N. Gong, W. Peng, Y. Li, F. Zhang and X. Fan, Boosting Zinc-Ion Storage in Hydrated Vanadium Oxides via Migration Regulation, *Energy Storage Mater.*, 2022, **55**, 279-288.

8. Y. Xu, G. Fan, P. X. Sun, Y. Guo, Y. Wang, X. Gu, L. Wu and L. Yu, Carbon Nitride Pillared Vanadate Via Chemical Pre-Intercalation Towards High-Performance Aqueous Zinc-Ion Batteries, *Angew. Chem. Int. Ed. Engl.*, 2023, **62**, e202303529.

9. Z. Zhang, B. Xi, X. Wang, X. Ma, W. Chen, J. Feng and S. Xiong, Oxygen defects engineering of $VO_2{\cdot}xH_2O$ nanosheets via in situ polypyrrole polymerization for efficient aqueous zinc ion storage, *Adv. Funct. Mater.*, 2021, **31**, 2103070.

10. Q. Zong, W. Du, C. Liu, H. Yang, Q. Zhang, Z. Zhou, M. Atif, M. Alsalhi and G. Cao, Enhanced Reversible Zinc Ion Intercalation in Deficient Ammonium Vanadate for High-Performance Aqueous Zinc-Ion Battery, *Nano-Micro. Lett.*, 2021, **13**, 116.

11. D. He, Y. Peng, Y. Ding, X. Xu, Y. Huang, Z. Li, X. Zhang and L. Hu, Suppressing the skeleton decomposition in Ti-doped $NH_4V_4O_{10}$ for durable aqueous zinc ion battery, *J. Power Sources*, 2021, **484**, 229284.

12. Q. Zong, Q. Wang, C. Liu, D. Tao, J. Wang, J. Zhang, H. Du, J. Chen, Q. Zhang and G. Cao, Potassium ammonium vanadate with rich oxygen vacancies for fast and highly stable zn-ion storage, *ACS Nano*, 2022, **16**, 4588-4598.

13. X. Wang, A. Naveed, T. Zeng, T. Wan, H. Zhang, Y. Zhou, A. Dou, M. Su, Y. Liu and D. Chu, Sodium ion stabilized ammonium vanadate as a high-performance aqueous zinc-ion battery cathode, *Chem. Eng. J.*, 2022, **446**, 137090.

14. Q. Sun, H. Cheng, Y. Yuan, Y. Liu, W. Nie, K. Zhao, K. Wang, W. Yao, X. Lu and J. Lu, Uncovering the Fundamental Role of Interlayer Water in Charge Storage for Bilayered $V_2O_5 \cdot nH_2O$ Xerogel Cathode Materials, *Advanced Energy Materials*, 2022, **13**.

15. Q. Sun, L. Chang, Y. Liu, W. Nie, T. Duan, Q. Xu, H. Cheng and X. Lu, Chrysanthemum-like Polyaniline-Anchored $PANI_{0.22} \cdot V_2O_5 \cdot 0.88H_2O$-Hybridized Cathode for High-Stable Aqueous Zinc-Ion Batteries, *ACS Applied Energy Materials*, 2023, **6**, 3102-3112.

16. Q. Sun, H. Cheng, C. Sun, Y. Liu, W. Nie, K. Zhao, X. Lu and J. Zhou, Architecting a Hydrated $Ca_{0.24}V_2O_5$ Cathode with a Facile Desolvation Interface for Superior-Performance Aqueous Zinc Ion Batteries, *ACS Applied Materials & Interfaces*, 2021, **13**, 60035-60045.